Transition Metal Dithiolene Near-IR Dyes and Their Applications in Liquid Crystal Devices

Introduction

The development of an ideal series of dyes for liquid crystal (LC) device applications represents a formidable synthesis challenge for chemists. To be considered useful for applications in LC devices, the class of dyes under consideration must have (1) a high solubility in the host matrix; (2) good long-term chemical, thermal, and optical stability; (3) low impact on the LC order parameter; (4) a large molar absorptivity; (5) low electrical conductivity; (6) large dichroic ratio; and (7) a λ_{max} located in the region of interest that can be tuned to some extent by relatively simple modifications in molecular structure. Dyes that possess all or nearly all of these properties are, for the most part, readily available for visible-region applications because of the large market for information display applications, which has provided incentive for the synthesis of a large number of highly suitable compounds. In comparison, the total range of dyes that are suitable for applications in the near-IR region is limited to around ten chemical classes. The majority of these dyes were designed for laser applications such as *Q*-switching and are either ionic or highly polar in nature and, thus, only soluble in polar solvents (e.g., acetone and methanol). Their solubility in LC hosts is very poor (around 0.01 to 0.05 wt%), which limits their potential absorption efficiency in an LC device to an optical density (OD) of <0.1 for a 25-μm material path length. Table 106.XI compares the physicochemical properties, solubility, and absorption characteristics of the currently known classes of near-IR absorbing dyes. Only five dye classes are soluble in nonpolar solvents and thus could be expected to show reasonable solubility in an LC

Table 106.XI: The properties of near-IR dyes evaluated as potential guest–host dopants for LC devices.

Dye class	Species	λ_{max} range (nm)	Solvents	Solubility in LC hosts (wt%)
Cyanine	Organic cationic	735 to 1100	Polar (acetone, methanol)	0.01 to 0.05 (*Q*-switch 5)
Azulenium	Organic cationic	728	Polar (acetone, methanol)	—
Pyrilium/ thiapyrilium	Organic cationic	748 to 879	Polar (acetone, methanol)	—
Iminium	Organic cationic	725 to 1090	Polar (acetone, methanol)	—
Squarilium/ croconium	Organic cationic	700 to 845	Polar (acetone, methanol)	—
Transition metal dithiolenes	Organometallic (zerovalent or anionic)	600 to 1600	Nonpolar (hexane, toluene)	10
Quinones/ anthraquinones	Organic zerovalent	748 to 810	Nonpolar (hexane, toluene)	2 to 3
Phthalocyanines	Organometallic zerovalent	630 to 830	Nonpolar (hexane, toluene)	—
Azo	Organic or organometallic zerovalent	700 to 900	Nonpolar (hexane, toluene)	2 to 3
Indoanilines	Organic zerovalent	660 to 800	Nonpolar (hexane, toluene)	—

host. Transition metal dithiolenes stand out as the most promising and interesting candidate of this group. They are highly soluble in nonpolar solvents (including LC hosts), their wavelength range spans from 600 nm in the visible to 1600 nm in the near IR (the latter wavelength is of special importance in military and telecommunications applications), and they possess excellent thermal and photochemical stability.

Interest in transition metal dithiolenes and their properties has been steadily increasing in recent years. They have been investigated as passive infrared absorbers for thermal imaging, photography, lithography, and electrophotography;[1] *Q*-switching–saturable absorbers for lasers,[2] optical limiters, and, in all-optical switching,[3,4] "unimolecular metals" exhibiting metal-like conductivity down to 0.6 K;[5] a "redox switch" for the binding and release of simple aliphatic olefins;[6] and as guest–host dyes for LC electro-optic devices for near-IR applications.[7,8] Earlier work by Muller–Westerhoff[9] and Ohta[10] established that these materials can possess numerous different stable LC phases depending on the structure of the terminal functional groups. This attribute was shown to be important for applications in LC guest–host systems since the presence of LC mesomorphism allows higher dye concentrations to be added to the LC host without substantially reducing its order parameter.[7,8]

In this article we present an overview of the physical and optical properties of transition metal dithiolene complexes that make them of special interest for near-IR applications in LC devices and discuss in detail our past and present research efforts in the design, synthesis, and characterization of both nonchiral and enantiomerically enriched forms of these interesting series of materials. The latter compounds are of special interest for device applications because of their low melting points (below room temperature in many cases) and ability to induce chirality in a nematic LC host when added as a dye dopant. As such, they could provide two separate modes of tunability when introduced into a liquid crystal material: (1) an electronic absorption mode that is tunable by alteration of the molecular structure through synthesis and (2) a selective reflection mode that is tunable by composition (concentration of the chiral dye in the host), electric field, and temperature. Some specific application examples for transition metal dithiolenes as near-IR dyes in LC electro-optical devices are also given. We conclude by presenting our most recent results that demonstrate the capability of computational chemistry to predict, prior to synthesis, both the near-IR electronic absorbance spectra and the helical twisting power (HTP) of transition metal dithiolenes as a function of molecular structure.

Properties of Transition Metal Dithiolenes

Transition metal dithiolene complexes[11,12] in which the central metal is in a zerovalent state (oxidation number = 0) exhibit strong absorption bands in the 600- to 1600-nm region of the spectrum and are highly soluble in nonpolar organic solvents (e.g., toluene and hexane) as well as LC materials. The central metal can be any transition metal capable of forming square planar complexes, but complexes based on nickel, palladium, and platinum are the most common. Figure 106.48 shows the generic molecular structure of the transition metal dithiolene core.

The strong near-IR absorption maximum observed in transition metal dithiolenes is a function of both extensive electron delocalization about the dithiolene ring system and the interaction of this delocalized system with available *d*-orbitals on the central metal (Fig. 106.49).[13] This interaction can be described using the linear combination of the atomic orbitals–molecular orbital (LCAO–MO) theory in which the atomic orbitals of the individual atoms are combined to form a series of lower-energy "bonding" and higher-energy "antibonding" molecular orbitals. The absorption of photons of sufficient energy results in the promotion of electrons from occupied (bonding) molecular orbitals to unoccupied (antibonding) molecular orbitals. The lowest-energy transition, and thus the one that occurs at the longest wavelength, is the transition between the highest occupied molecular orbital (HOMO) and the lowest unoccupied molecular orbital (LUMO) and is referred to as the "band gap." This HOMO–LUMO transition is the one responsible for the strong near-IR absorption in the transition metal ditholenes.[11,13] A secondary electronic transition of weaker energy also occurs in the visible region between 500 and 600 nm in these materials. A change in the oxidation state of the metal eliminates the near-IR absorption, greatly strengthens absorption in the visible region, and renders the complexes soluble only in polar solvents. Substi-

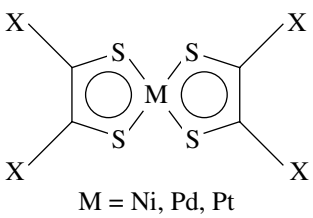

Ph =

where X = H and R = C_nH_{2n+1}
Ph OC_nH_{2n+1}
PhR $N(CH_3)_2$
SR

Figure 106.48
The general molecular structure of transition metal dithiolenes. The physical properties of the complex are determined by the nature of the terminal functional groups, designated as X.

tution of the central metal with a different zerovalent transition metal also produces changes in the near-IR λ_{max}. Platinum and palladium complexes show a 20- to 30-nm hypsochromic (blue) shift and bathochromic (red) shift, respectively, as compared to nickel complexes with the same ligand structure.

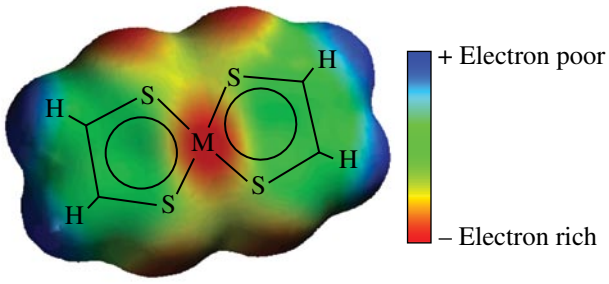

Figure 106.49
Ground-state charge distribution map of the nickel dithiolene core. The sulfur and nickel atoms are the most electron-rich areas in the molecule.

The nature of the functional groups attached to the metal dithiolene core has a large effect on both the position of the electronic absorption maximum and the solubility of the dye in the host matrix. Conventional wisdom teaches that the best way to shift the electronic absorption maximum to longer wavelengths is to maximize the extent of electron delocalization by utilizing aromatic ring structures with an extensive π-delocalization capability (phenyl, naphthyl, and anthracenyl) either as functional groups or incorporated within the central core of the molecule. Although effective, this approach has the dual disadvantage of increasing the melting point of the complex while decreasing its solubility. Counterintuitively, we found that thioether groups bonded directly to the dithiolene core not only shift the near-IR absorption of the complex to longer wavelengths but also *enhance* their solubility in LC hosts. As a direct result of this finding, we focused our attention on preparing new transition metal dithiolene complexes based on thioether terminal groups. Because platinum dithiolene complexes absorb at shorter wavelengths and palladium complexes have proven to be very difficult to synthesize and isolate in a form pure enough for device applications, we continued to use nickel as the central metal of choice for these new materials.

Absorbance Dichroism

Transition metal dithiolenes are excellent candidates for near-IR guest–host devices because of their high molar absorptivity (>30,000), remarkable thermal and photochemical stability, and high solubility in LC hosts as compared to other near-IR dyes. Figure 106.50 (top) shows the field-induced dichroism of a mixture of 1% of the nematic liquid crystalline metal complex "BisBuSDNi" in the nematic LC K-15 measured in a 24-μm-thick, antiparallel-rubbed cell with (1) no field applied and (2) a 10-V, 100-KHz square wave applied to switch the cell into the homeotropic orientation. The drop in absorbance indicates positive dichroism; the contrast ratio at 860 nm is 5:1. An OD of 2.4 is easily achievable in the off state, and OD's of 3.5 have been measured in similar cells at higher dye concentrations.[7]

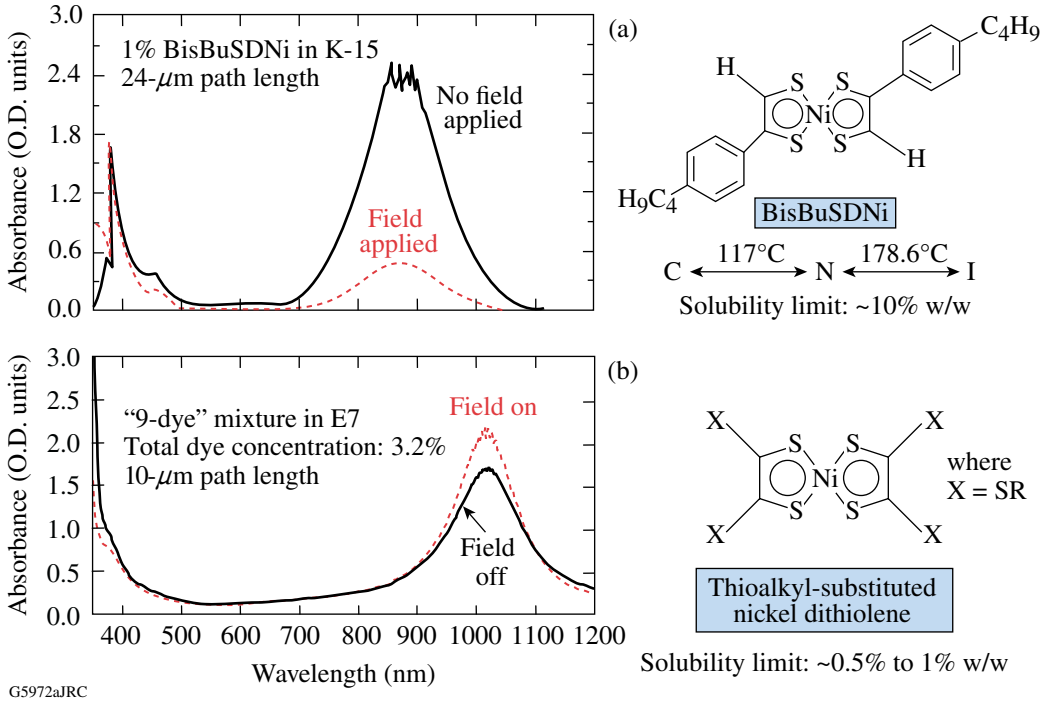

Figure 106.50
(a) Change in absorbance with applied voltage for a 1% concentration of "BisBuSDNi" in a 24-μm-thick, antiparallel-rubbed cell. An OD of 3.5 at 860 nm is achievable at higher dye concentrations. (b) Field-induced dichroic behavior of a mixture of nine thioalkyl-substituted nickel dithiolene dyes in Merck E7. Increasing the number of terminal substituents from two to four and altering their structure changes the sign of the dichroism from positive to negative.

Changes in molecular structure can cause substantial changes in both the position of the dye λ_{max} and the nature of the field-induced dichroism. Figure 106.50 (bottom) shows the field-induced behavior of a mixture of nine thioalkyl-substituted nickel dithiolene dyes in Merck E7. The total dye concentration was 3.2%, and the cell path length was 10 μm. This new series of dyes shows a small degree of *negative* dichroism, whereas the materials synthesized previously showed only *positive* dichroism.

Solubility in an LC Host

Solubility testing of thioalkyl-substituted nickel dithiolene dyes in the LC host E7 (Merck) was conducted at selected concentrations between 0.3 wt% to 1 wt% along with several phenyl-substituted nickel dithiolenes as reference compounds. Each dye was dissolved into 2 ml of the host by heating the host/dye mixture to 100°C with stirring for several hours. Upon cooling, each sample was filtered through a 0.45-μm Teflon membrane filter to remove any insoluble material. All samples were checked daily, both visually and by microscopic inspection at 100× magnification, for evidence of dye precipitation. For samples that showed precipitation, new mixtures were prepared at lower concentrations until a stable dye concentration was achieved.

Computational chemistry methods were employed in a parallel and complementary effort to aid in predicting the appropriate functional group combinations that would yield materials with the desired solubility and spectroscopic parameters.[14] Because limitations in the computational methods precluded solubility calculations in either anisotropic solvents or solvent systems composed of mixtures of compounds, Merck CB-15, an isotropic chiral cyanobiphenyl compound, was used to establish *qualitative* solubility trends.

The solubility of a given solute in a solvent can be approximated by calculating its solvation energy and comparing this value with the bonding, or "reorganization," energy. The solvation energy ΔG_{solv} is defined as[15]

$$\Delta G_{solv} = \Delta G_{elec} + \Delta G_{cov} + \Delta G_{disp} + \Delta G_{vib} + \Delta G_{lib} + \Delta G_{other}, \quad (1)$$

where ΔG_{solv} is the solvation energy, ΔG_{elec} is the electrostatic solute–solvent interaction, ΔG_{cov} is the energy to form a solute-shaped cavity, ΔG_{disp} is the London and van der Waals interactions, ΔG_{vib} is the change in vibrational energy due to damping, ΔG_{lib} is the conversion of rotations and translations to librations, and ΔG_{other} is the solvent enthalpic and entropic structure (PV term, etc.). The value ΔG_{solv} can be used as a qualitative indicator of general solubility of the dye solutes in the same host with a larger positive value generally indicating a greater solubility in the solvent host matrix. Table 106.XII gives a compilation of melting points, near-IR absorbance, and solubility (calculated versus experimental results) for a series of substituted nickel dithiolene complexes with substituted phenyl and alkylthio terminal groups. General trends that can be drawn from the data in Table 106.XII are, that as the terminal groups are changed from substituted phenyl to alkylthio, (1) the melting points of the complexes drop drastically, (2) the near-IR λ_{max} of the complexes are shifted substantially to longer wavelengths,

Table 106.XII: Comparison of melting points, near-IR absorbance maxima, and solubility data (both calculated and experimental) for a series of phenyl-substituted and alkylthio-substituted nickel dithiolene dyes in Merck CB-15 and E7 hosts. A larger *positive* value for ΔG_{solv} indicates higher solubility.

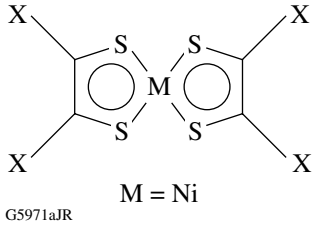

Terminal (X) group	Melting point (°C)	λ_{max} in E7 (nm)	CB-15		Merck E7
			Solubility limit (wt%)	ΔG_{solv}	Solubility limit (wt%)
$-SC_8H_{17}$	73	1020	1.0	–7.6725	0.50
$-SC_7H_{15}$	81.5	1020	0.5 to 1.0	–7.7164	0.50
$-SC_4H_9$	101	1020	0.5 to 1.0	–7.7190	0.50
$-PhC_4H_9$	228 to 230	910	0.3 to 0.5	–14.4373	0.50
$-PhN(CH_3)_2$	280 to 283	1056	0.3 to 0.5	–17.4080	0.05
$-PhOC_9H_{19}$	184 to 189	970	0.1 to 0.3	–21.6724	0.30
$-PhOC_4H_9$	246 to 248	970	0.1 to 0.3	–21.6950	0.30

and (3) the solubility of the complexes in both CB-15 and E7 (both calculated and experimental) increases.

Materials Synthesis

The synthesis of nickel dithiolene dyes and their precursor ligands was conducted using modifications of literature methods and have been reported elsewhere. Three basic methods have been employed, depending on the degree of substitution desired in the complex and its overall symmetry. Mesogenic nickel dithiolenes were synthesized by a modification[7] of an earlier three-step procedure reported by Mueller–Westerhoff *et al.*,[9,11] as shown in Fig. 106.51. Although relatively simple, this method has some disadvantages in that the products are difficult to separate from the tarry by-products formed from phosphorous pentasulfide and, as a result, the yield of purified product is very low (5% to 15%). A second method that is useful for the preparation of alkylthio-substituted nickel dithiolenes is based on literature methods reported by Wainwright and Underhill,[16] N. Svenstrup *et al.*,[17] and A. Charlton *et al.*,[18] as shown in Fig. 106.52. The method

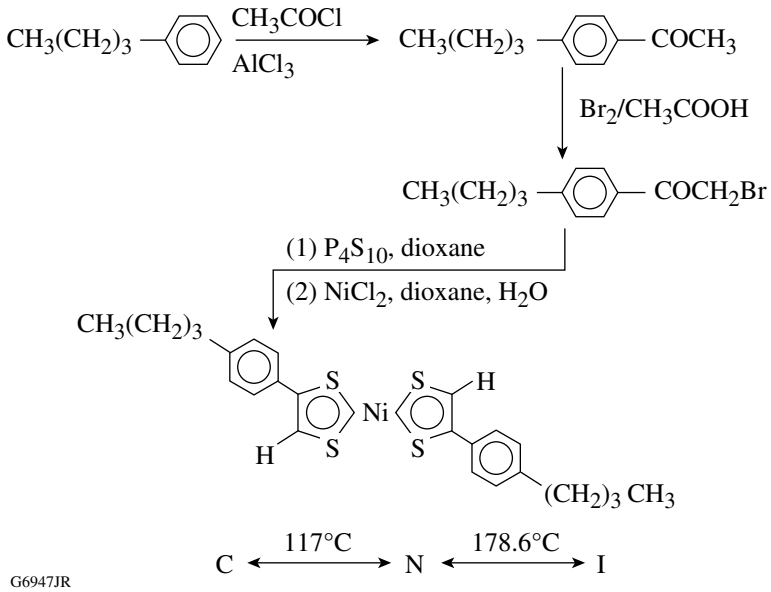

Figure 106.51
The synthesis method for rod-like nickel dithiolene compounds possessing a liquid crystal phase.

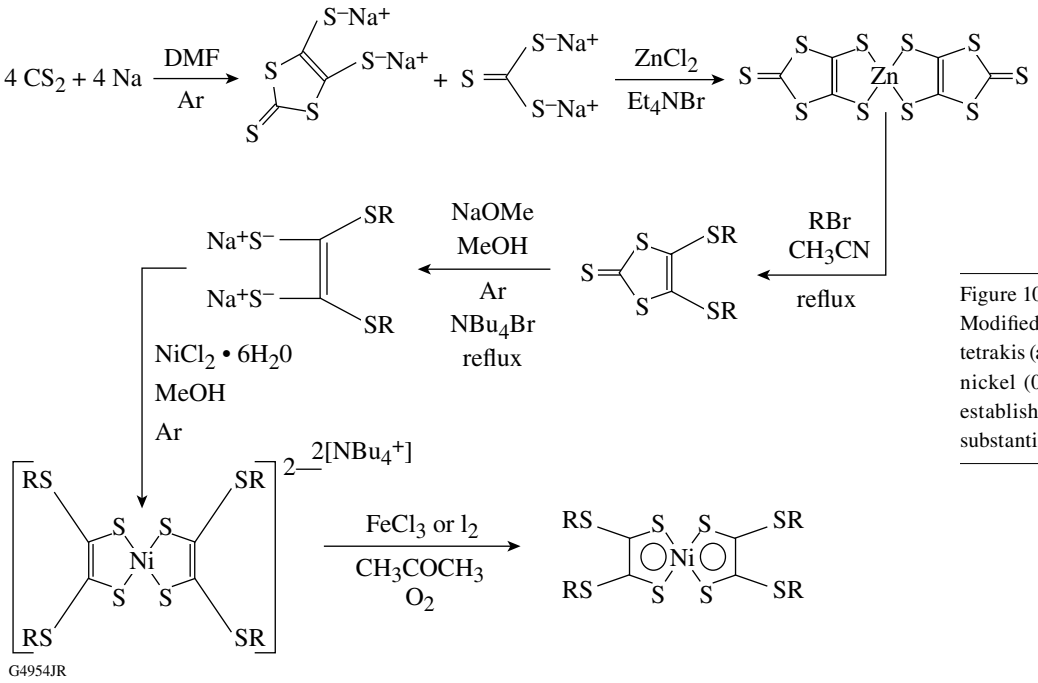

Figure 106.52
Modified synthesis scheme for preparation of tetrakis (alkylthio) bis(ethylene-1,2-dithiolene) nickel (0) complexes. Modifications to the established literature procedures resulted in substantially improved yields of product.

is applicable to both chiral and nonchiral terminal groups. For nonchiral terminal groups, yields of the complexes ranged from 27% to 68%, while yields of complexes with bulkier, enantiomerically enriched terminal groups were substantially lower (5%–10%). A third method allows the insertion of a flexible alkyl spacer ranging from 2 to 9 carbons between the thio group attached to the dithiolene core and an enantiomerically enriched chiral terminal group based on nonracemic carboxylic acids or alcohols, as shown in Fig. 106.53. The large, flexible, and bulky terminal groups make them somewhat difficult to isolate and purify. Currently, the overall yields for these materials are quite low, ranging from a few percent up to around 15% for materials with shorter alkyl spacer groups.

Enantiomerically Enriched Nickel Dithiolene Complexes

Table 106.XIII gives the generic structure and physical properties, respectively, of these nickel dithiolene complexes with enantiomerically enriched terminal groups. The most remarkable feature of this series of chiral materials is how rapidly and dramatically their melting points decrease as the length and breadth of the terminal groups increase. With the exception of the S-(+)-2-methylbutylthioether derivative, all of the other materials are liquids at room temperature.

Another interesting attribute of these new chiral metal dithiolenes is that they are capable of inducing a chiral nematic phase when added to a nematic LC host. Figure 106.54 shows

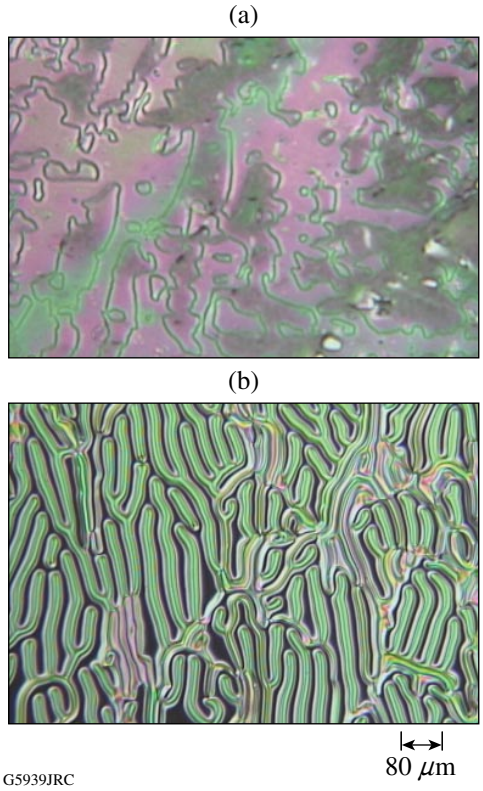

Figure 106.54
Chirality transfer to an LC host by doping with a chiral nickel dithiolene complex. (a) Pure Merck E7 and (b) Merck E7 containing 0.5% of the S-(+)-2 methylbutyltioether-substituted nickel dithiolene.

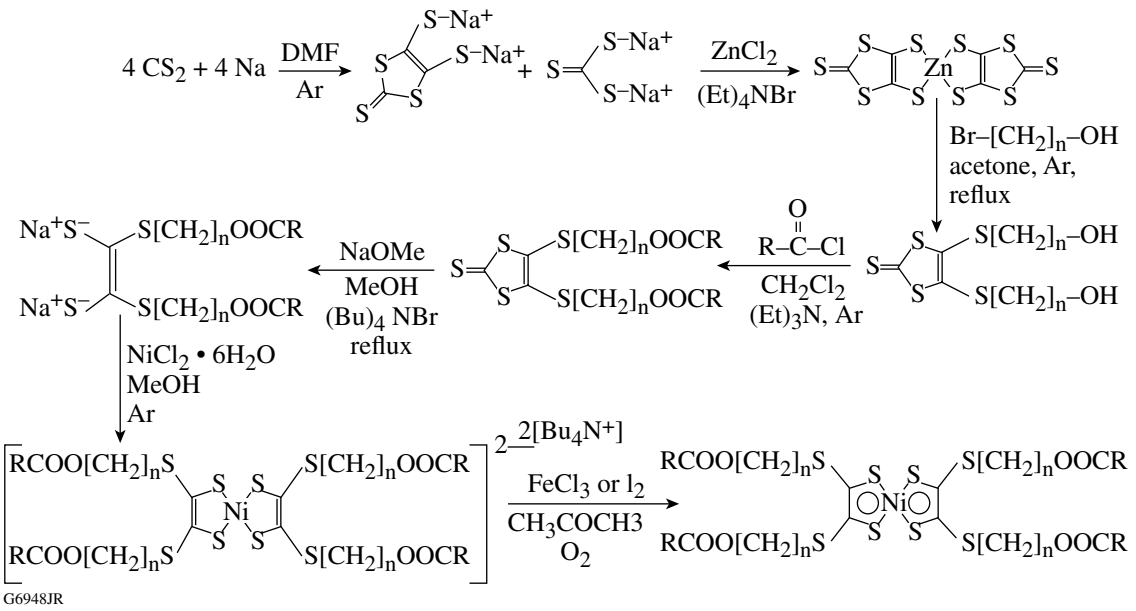

Figure 106.53
Synthesis scheme for chiral transition metal dithiolenes incorporating a flexible spacer between the terminal groups and the dithiolene core.

photomicrographs under crossed polarizers of a sample of Merck E7 before and after doping with 0.5% of the S-(+)-2 methylbutylthioether-substituted nickel dithiolene. The fingerprint texture generated in the doped sample (helical pitch, length = 80 μm) is clear evidence that the chirality of the metal complex has been transferred to the LC host.

Device Applications

Transition metal dithiolenes have many possible commercial, military, and scientific applications in LC electro-optical devices for the near-IR region. Their high solubility in LC hosts, capability of exhibiting mesomorphism, excellent thermal and photochemical stability, dichroic capability, and broad wavelength range have

Table 106.XIII: Physical properties of the new chiral nickel dithiolene complexes.

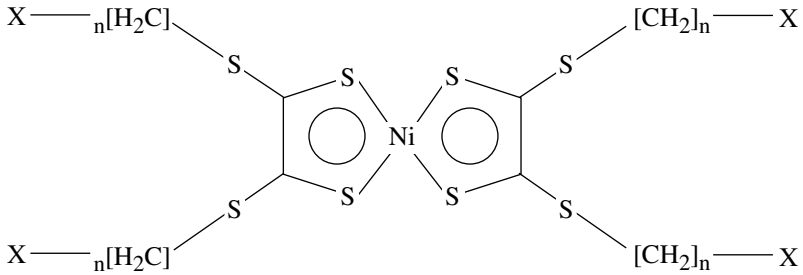

X group	Spacer (*n*)	MP (°C)	λ_{max} (nm) (a) E7 (b) Toluene	Helical pitch length (E7, μm)
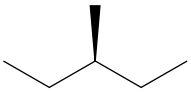	0	108.5	1020[a]	80
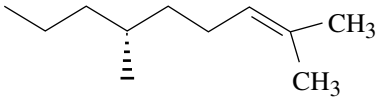	0	–43	1020[a]	30
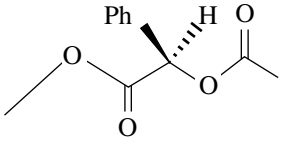	3	–45	1009[b]	
	6	–50	1009[b]	
	9	–49	1009[b]	
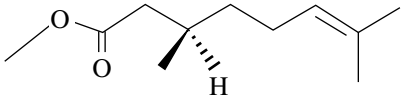	3	<25	1008[b]	
	6	–46	1008[b]	
	9	–46	1008[b]	
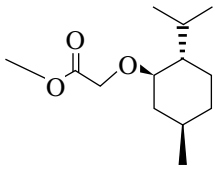	3	–52	1005[b]	
	6	–45	1005[b]	
	9	–46	1010[b]	
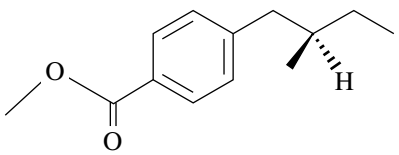	3	<25	1011[b]	
	6	–52	1011[b]	
	9	<25	1011[b]	

G5973JR

made them of interest for use in LC devices for near-IR optical modulation, switching, nonlinear optics, and sensor protection.[14] In addition to these applications, nonchiral nickel dithiolenes have been extensively investigated as a component of the liquid crystal point diffraction interferometer (LCPDI), a phase-shifting, common-beam-path interferometer that uses an LC electro-optic device as the modulation element.[19,20] Because both the object and reference beams follow the same path, the LCPDI is relatively insensitive to the mechanical vibrations, temperature fluctuations, and air turbulence that plague conventional phase-shifting interferometers. The LC host used in the LCPDI must be doped with a dye to compensate for differences in the cross sectional area of the sample and reference beams to ensure good fringe contrast (Fig. 106.55). Ideally, the dye should have as low a dichroism as possible to maintain constant interference fringe contrast with applied voltage. The LCPDI is being investigated as a beamline diagnostic for the 60-beam, 40-TW, 1054-nm OMEGA Laser System used in the Department of Energy's inertial confinement fusion research at the Laboratory for Laser Energetics. The large physical size and the need for vibration isolation make conventional near-IR phase-shifting interferometers impractical for these characterization activities since each of the 60 beams would have to be propagated a long distance across free space to reach the interferometer table. To date, transition metal dithiolenes are the only class of near-IR dyes that have the necessary combination of physical properties suitable for a near-IR LCPDI device.

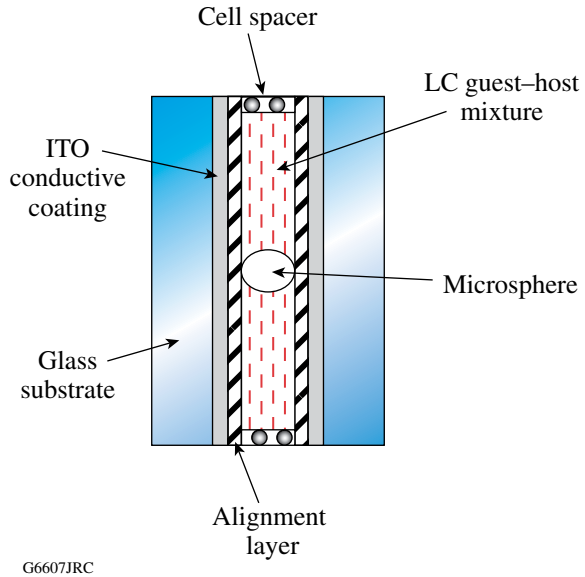

Figure 106.55
A schematic representation of the liquid crystal point diffraction interferometer (LCPDI) device.

The addition of chirality to the dithiolene core now opens new application possibilities. Since these new materials are noncentrosymmetric, they may exhibit interesting nonlinear optical properties, either on their own in the liquid state or as a dopant in a suitable host. The demonstrated induction of chirality in nematic phases by doping with a chiral nickel dithiolene suggests the possibility of devices for sensor protection in the near IR that have two modes of tunability: one mode through the absorbance of the nickel dithiolene dye (tunable by synthesis) and a second tunable mode employing selective reflection wavelength shifting induced by electric field or temperature changes (see i.e., Fig. 106.56).

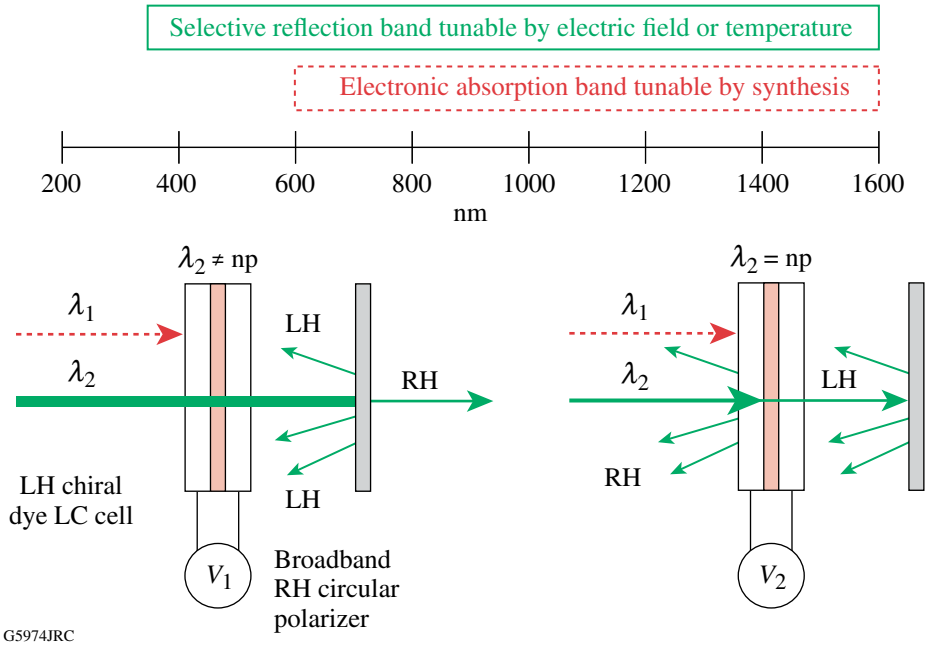

Figure 106.56
Device concept for sensor protection in the near IR based on chiral nickel dithiolene dyes. The device has two modes of tunability: one mode through the absorbance of the nickel dithiolene dye (tunable by synthesis) and a second tunable mode employing selective reflection wavelength shifting induced by electric field or temperature changes. Selective reflection occurs when the incident wavelength λ equals the product of the average refractive index of the LC material and its pitch length P.

Computational Chemistry Modeling of Nickel Dithiolene Systems

Advances in the science of computational chemistry over the past 20 years, the widespread availability and increasing ease of use of computational chemistry software, and an exponential reduction in the cost and size of extremely powerful computer hardware now make some degree of computational predictive capability for physical properties (e.g., solubility, electronic and vibrational spectra, reactivity, molecular configuration, and chirality) within the reach of nearly every laboratory that is involved in new materials research and development. Previously and out of necessity, researchers would have to follow an empirical approach of synthesizing, isolating, characterizing, and purifying hundreds of different compounds to establish structure–property relationships that could be used to further direct the design and development effort toward the desired goal. Of these hundreds of compounds synthesized, only a handful would have the necessary combination of physical characteristics to be deemed worthy of further study and development. Such a process is not only time consuming, labor intensive (weeks to months to completely synthesize and characterize each compound), and costly, but can also be highly frustrating for organic chemists engaged in the synthesis of new materials—especially for those with limited resources. Modern hardware and user-friendly software now make it possible to model new compounds and their physical properties with remarkable accuracy within a few hours or days, which only a few years ago would have taken from weeks to months of work to achieve the same results.

Nowhere has there been more evidence of the predictive capability of computational chemistry than in the pharmaceutical industry, where computational molecular design techniques have been used to great advantage for a number of years in the rapid development of new drugs with enhanced biological activity and specificity at lower cost. More recently, computational chemical methods have been applied to the molecular engineering and design of liquid crystal materials for use both in the multibillion dollar information display industry and the optoelectronic, photonics, military, and life sciences sectors. In all of these examples, the vast majority of the target materials systems consist of *organic molecules* composed mainly of carbon, hydrogen, and nitrogen in combination with a few other elements (e.g., sulfur, fluorine, and phosphorous). The state of the art in computational chemistry modeling in these materials is well developed, and computational algorithms and procedures are well defined in a large body of existing literature. The application of computational chemistry techniques to transition metal organometallics and particularly the transition metal dithiolenes, represents a substantial challenge mainly for several reasons that include (1) the lack of previous research activity in the area from which to draw direction from, (2) the extremely small number of parameter files (basis sets) that can adequately account for the unique nature of the coordinate-covalent bonds that are formed in these materials, (3) the intensive computational resources required to accomplish the calculations, and (4) the scarcity of computational chemistry software capable of modeling organometallic systems. In what follows, we describe the computational modeling methodology that we have developed and applied to nickel dithiolene systems to predict, prior to synthesis, properties that include (a) the near-IR electronic absorbance spectra and (b) the helical twisting power (HTP) of the nickel dithiolene complex in a host medium for enantiomerically enriched materials. This effort is believed to be the first time that such calculations of this nature have been attempted in nickel dithiolene systems or in any other transition metal organometallic complex.

1. Modeling of Electronic Transitions States and Near-IR Absorbance Spectra

The process of modeling electronic absorbance spectra is composed of three key steps.

- *The free energy of the molecular structure with respect to its conformation is minimized.*

Molecular mechanics calculations employing Newtonian mechanics and empirical force fields are used to generate a particular molecular conformation that represents an energy-minimized state with respect to bond angles, electrostatic repulsions, and steric factors. This energy-minimized structure represents an approximate equilibrium conformation that must be further refined using quantum mechanical methods.

- *The electron distribution in the molecule is determined, and the available electronic energy levels and excited states are calculated.*

Either semiempirical or *ab initio* quantum mechanical methods can be used for this task. Semiempirical methods use some approximations and are employed when a certain degree of computational accuracy can be sacrificed in exchange for reduced computational resources and run time. *Ab initio* methods provide a much more detailed and accurate description of the quantum mechanical aspects of a molecular structure but do so at a cost of increased computational resource requirements and time. The substantially improved accuracy of *ab initio* calculations made them the preferred method for modeling the

exceedingly complex electronic distribution and excited-state transitions found in nickel dithiolenes.

Ab initio calculations are based on a detailed description of the quantum mechanical aspects of a molecular structure using the Schrödinger equation, defined as

$$H_{\text{op}}\Psi = E\Psi, \tag{2}$$

where H_{op} is defined as the Hamiltonian operator, Ψ as the wave function of the system, and E as the energy of the system. The Hamiltonian of the system represents its kinetic and potential energy. In a three-dimensional system, the Hamiltonian operator is defined as

$$H_{\text{op}}\Psi = \frac{-h^2}{2m}\left(\frac{\partial^2\Psi}{\partial x^2} + \frac{\partial^2\Psi}{\partial y^2} + \frac{\partial^2\Psi}{\partial z^2}\right) + U\Psi, \tag{3}$$

where h is Planck's constant divided by 2π and m is the mass of an electron. The terms x, y, and z are the Cartesian coordinates of an electron with respect to the nucleus, while U refers to the potential energy of the system.[21]

A wave function is a mathematical expression that describes the wave nature of an electron after certain restrictions are placed on it by basis sets, which give specific information on the electronic structure and orbitals of the atoms as well as describing the path and behavior of electrons. The wave function expression is a group of Gaussian-type orbital equations for which the generic equation is

$$\Psi = Nx^l y^m z^n e^{-\alpha r^2}, \tag{4}$$

where x, y, and z are the Cartesian coordinates; l, m, and n are positive integer values that describe the angular momentum of the orbital, r is the distance to the center of the atom, N is the normalization constant, and α represents the orbital exponent of the Gaussian function.

Because the Schrödinger equation cannot be solved directly for a many-electron system, various approximation methods can be used to make it solvable. The Hartree–Fock method uses three approximations to estimate the many-electron wave function; these include (1) the *Born–Oppenheimer approximation* (assumes that all nuclei are motionless with respect to the electron), (2) the *linear combination of atomic orbitals (LCAO) approximation* (assumes that electron orbitals may be expressed as one-electron basis functions centered on each atom), and (3) the *Hartree–Fock approximation* (which assumes that the sum of all single-electron calculations of a molecule is the same as the multi-electron calculation of the molecule). Because of inaccuracies associated with the Hartree–Fock approximation, the entire Hartree–Fock computational method becomes less accurate with increasing molecular size.[22]

Unlike the Hartree–Fock method, which uses an exact Hamiltonian with approximate wave functions written in terms of a product of one-electron functions, the density function theory (DFT) method replaces the many-electron wave function with electronic density as the basic quantity.[23] The DFT method is widely employed in the field of computational chemistry and is considered to be a good method to use with transition metal complexes.

- *Calculation of the allowable ground-state to excited-state transitions that are responsible for the electronic absorbance spectrum.*

The expected excited-state electronic transitions are determined by including the configuration interaction (CI) model in the *ab initio* quantum mechanical calculations. The CI model is derived from Hartree–Fock calculations that are expanded to incorporate electronic excitation and changing shell levels.

Because there was no single software package capable of handling all of the computational tasks, a total of four separate software packages running on two different computing platforms were required. Molecular mechanics computations were conducted using Spartan 4 (Wavefunction, Inc.) on a 2-Ghz, dual-processor Intel XEON server. *Ab inito* and electronic spectra calculations were conducted using the open-source computational package GAMESS (General Atomic and Molecular Electronic Structure System) from Iowa State University on a SGI Altix Server using sixteen 2.5-GHz Itanium 2 processors. Input-to-output file format conversions from Spartan to GAMESS were accomplished using Open Babel (www.sourceforge.net), while the final spectral output from GAMESS was processed, displayed, and plotted using the WebMO graphical user interface (http://webmo.net/index.html).

Specifying the appropriate conditions to conduct the *ab inito* calculations using GAMESS proved to be extremely challenging. Parameter options and appropriate basis sets for the calculations must be selected and specified properly to achieve valid results. For relatively small organic molecules there is existing literature to guide the selection of appropriate options and parameter sets, but in the case of nickel dithiolenes

there is no pre-existing body of literature from which to draw guidance. The proper calculation conditions were determined through a combination of (1) an extensive study of the general literature on *ab inito* molecular modeling theory, (2) review of the handful of existing references on *ab inito* modeling in unrelated transition metals and their complexes, and (3) testing the selected modeling parameters and conditions by means of an iterative trial and error process. The calculation options that were ultimately selected and used in testing the model and its application to new nickel dithiolene systems are

- *SCFTYP (self-consistent field wave function):* Specifies the basic calculation type that is used. For our work, the restricted Hartree–Fock[24] (RHF) and density functional theory[25] (DFT) options were used. The RHF method was ultimately chosen for the final calculations because (1) it was found to be more accurate than the DFT method in initial test trials, and (2) since the CI calculations required to calculate the absorbance spectra are based on the RHF calculations, they cannot be run concurrently with the DFT option.

- *CITYP (configuration interaction model type):* Includes and specifies CI models in the *ab initio* calculations for electronic spectra calculations.

- *BASIS and GBASIS:* Specifies the type of basis set used for the calculation and what type of basis set function to choose, respectively. The minimal basis sets (GBASIS = STO) and split-valence basis sets (GBASIS = N31) were chosen initially because they were one of the few basis sets that were capable of producing accurate calculations for the electronic structure of nickel dithiolenes. The minimal basis set used was STO-3G (Refs. 26 and 27) with three Gaussian functions. Split-valence basis sets used were 6-31G with six Gaussian functions, and 6-31G(d) (Ref. 28) with both six Gaussian functions and functions that included *d*-orbital calculations. The split-valence basis sets proved to be more accurate because they correctly predicted that valence electrons do most of the bonding. The 6-31G(d) basis set specifies the inclusion of *d*-orbitals in the calculations, thus increasing their accuracy.

- *SCF and DIRSCF:* Specifies whether the self-consistent field wave function will be calculated directly or indirectly.[29] Hartree–Fock calculations make use of a large number of two-electron repulsion integrals that are stored and retrieved from hard disk storage. The direct SCF calculation re-evaluates the integrals directly without storing to disk during each Hartree–Fock iteration, which dramatically speeds up processing time.

- *CIS and NSTATE:* Specifies the method for determining the electronic structure[30] and how many different peaks in the electronic spectrum should be selected for the calculations, respectively. The optimal value for NSTATE was 10, as lower values would generate inaccurate results while higher values would significantly increase calculation times without any significant gain in accuracy.

- *DAMP:* Aids in allowing the system to converge to an energy minimum state during SCF calculations.[31,32] *Ab initio* calculations were found to fail consistently in nickel dithiolene systems unless this option was added.

The accuracy of the computational method was tested by modeling a series of nickel dithiolenes reported previously in the literature by Mueller–Westerhoff *et al.*,[13] calculating the expected near-IR absorbance spectrum and comparing the resultant values to the literature data in several different solvents (Table 106.XIV). A Pearson correlation *r* (a measure of the fit of a least squares linear regression through the data set) between the calculated and experimental near-IR absorbance data was determined for the compounds in Table 106.XIV. The correlation coefficient R^2 describes the proportion of the points that can be accounted for by the linear regression. For the near-IR absorbance data in Table 106.XIV, a correlation coefficient

Table 106.XIV: Calculated and experimental near-IR peak absorbance data for a series of nickel dithiolene compounds previously prepared and reported in the literature.

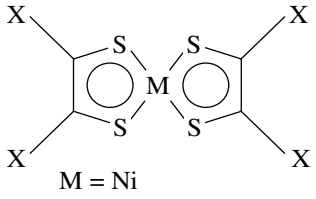

G6945JR

Terminal group	Experimental solvent	Experimental wavelength (nm)	Calculated wavelength (nm)
X = H	Hexane	720	720.91
X = CH_3	$CHCl_3$	774	843.08
X = CF_3	Pentane	715	775.05
X = S-C_4H_9	$CHCl_3$	1104	1012.31
X = C_6H_5	$CHCl_3$	866	845.19
X = 2-napthyl	$CHCl_3$	905	993.08
X_1,X_4 = H X_2,X_3 = C_6,H_5	CH_2Cl_2	805	857.78

of 0.910117443 was obtained, which represents an excellent correlation between calculated and experimental results for a majority of the compounds modeled, considering that the theoretical model assumes that the molecule is not solvated (i.e., in a vacuum). The excellent correlation is strong evidence of the predictive capability of the computational method and validates its use in predicting electronic transition states in nickel dithiolene systems that have yet to be synthesized.

Table 106.XV shows the results obtained when the new computational method was applied to a series of yet-to-be synthesized nickel dithiolene systems with ligands of varying structure. The goal of this exercise was to be able to establish structure–property relationships that could be used in the design of new materials with an advantageous combination of physical and optical properties (high host solubility, large absorbance oscillator strength, and control of the peak absorbance maximum) through ligand selection. One nickel dithiolene complex with C_6 alkyl terminal groups that has been previously prepared is also included in the table as a reference. One significant trend that can be observed on examination of the table is that the near-IR peak wavelength is red-shifted when sulfur-containing groups are bonded directly to the dithiolene core, whereas for phenyl groups the near-IR maximum is blue-shifted. This observed trend is somewhat counterintuitive as it is normally accepted that the addition of aromatic groups in conjugation with another aromatic structure generally shifts the absorbance maximum of the molecule to *longer* wavelengths than do alkoxy or thioakyl groups because of resonance stabilization (the energy gap between electron levels is reduced, thus allowing electronic-state transitions to occur at a lower energy and longer wavelengths). Clearly, the *d*-orbitals on the sulfur-containing terminal groups are providing a greater degree of resonance stabilization in this case than the phenyl groups. The nature of this stabilization is not yet understood and will be investigated in the future.

Table 106.XV: Predicted electronic spectral maxima for a series of candidate nickel dithiolene compounds that have yet to be synthesized. The first entry in the table is a compound that has been synthesized and included for reference.

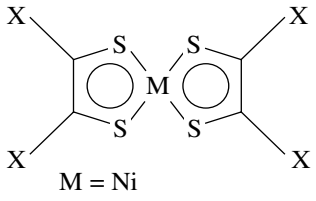

Terminal groups	Experimental wavelength (nm)	Predicted wavelength (nm)
$X = C_6H_5$	866	845.19
X = S-H		1053
X = S-Ph		972
X_1,X_4 = S-H X_2,X_3 = S-Ph		1004
X_1,X_4 = H X_2,X_3 = S-Ph		1038
X_1,X_4 = H X_2,X_3 = S-H		1055

A serious limitation of the current modeling method is that GAMESS appears to be unable to produce accurate electronic spectral data for nitrogen-containing compounds. Computational failures were routinely encountered in every attempt to model nitrogen-containing nickel dithiolene structures. The same results were obtained in attempts to model even very simple, classical nitrogen-containing organic compounds. The source of the problem at this point is still unresolved, but it appears to be a basic functional issue with GAMESS itself and not with our specific computational methodology or parameter files. An investigation of this issue is ongoing.

2. Modeling of Chirality and HTP

In an effort to gain a better understanding of the relationship between absolute molecular configuration and optical rotation direction, there has been increasing interest in representing chirality in a more quantitative, mathematical manner. It is somewhat surprising that the computational prediction strategy so successfully exploited by the pharmaceutical industry has only been applied very recently to the prediction of "chiroptical" properties of LC systems for advanced optical and photonics applications. The earliest reported activity in this area was by Lisetski *et al.*,[33–35] who used atomic coordinates determined either experimentally by x-ray diffraction or computationally from molecular models to calculate the HTP for a series of cholesteryl esters.

More recently, chirality has been determined computationally using two different approaches that are innately different in their level of development, ease of use, and efficiency. The first of these methods, explored in 1995 by Zabrodsky *et al.*,[32,36] attempts to find the absolute distance between the corresponding atoms of the two configurations of a chiral molecule if they were to be superimposed over one another. One disadvantage

of this method is that it is extremely computationally intensive because of the large number of iterations required to arrive at solutions that are meaningful.

In 1995 Osipov *et al*.,[37] building on the work of Listeski *et al*,[33–35] proposed a second, simpler method based on the calculation of a "figure of merit" for chirality that they termed the chirality index (G_0). Recently, Solymosi *et al*.[38] improved upon the chirality index by introducing a scaling factor that allows comparison between molecules with different numbers of atoms. This scaled chirality index (G_{0S}) is used to find the contributions of individual atoms and atom groups to the overall (global) chirality of the molecule. This scaled chirality index is useful even in its abstract form; any asymmetry, if it exists, will be revealed by the nonzero value of G_{0S}. A symmetrical molecule returns a chirality index value of zero in nearly every case. Promising correlations between G_{0S} and important applications properties such as circular dichroism (CD) and the HTP of a chiral dopant in a liquid crystal host also have been shown by Neal *et al*.,[39] and Osipov and Kuball.[40]

The scaled chirality index can be used to compare molecules of different sizes and is constructed to be maximized for a molecule with a strong steric stress and to vanish for any molecule that contains the point symmetry element S_n (a rotation-reflection axis), which would preclude chiral behavior. The chirality index is also capable of predicting the sign of the optical activity.

The numerical expression for the scaled chirality index is

$$G_{0S} = \frac{4!}{N^4}\frac{1}{3}\left\{\sum_{\substack{\text{all permutations of}\\ i,j,k,l=1}}^{N} w_i w_j w_k w_l \times \frac{\left[\left(\mathbf{r}_{ij}\times\mathbf{r}_{kl}\right)\times\mathbf{r}_{il}\right]\left(\mathbf{r}_{ij}\times\mathbf{r}_{jk}\right)\left(\mathbf{r}_{jk}\times\mathbf{r}_{kl}\right)}{\left(r_{ij}r_{jk}r_{kl}\right)^n r_{il}^m}\right\}, \quad (5)$$

where $\mathbf{r}_{ij}$ values are the atomic radii of the atoms contained in the chiral group upon which the chirality calculations are conducted and w_i, w_j, w_k, and w_l are values that represent the weighting factors of the individual atoms i thru l. We used this numerical expression to develop a multiplatform, multithreaded computational program to efficiently compute the chirality index for molecules of up to 250 atoms within minutes on most high-performance computer systems. Initial computations were performed on a SGI Origin 2000 server (sixteen 400-MHz processors) running SGI IRIX 6.5, which would typically complete a chirality index calculation for a molecule with 200 atoms in approximately 4 h. The same code recompiled to run on a SGI Altix server (sixteen 2.5-GHz Itanium 2 processors) running Red Hat Enterprise Linux Release 3 computed the chirality index for the same compound with 200 atoms in approximately 5 min.

Finally, using the scaled chirality index, it is possible to determine the contributions of each atom to G_{0S} using

$$G_{0SA} = G_{0S} - \frac{4!}{N^4}\frac{1}{3} \times \left\{\sum_{\substack{\text{all permutations of}\\ i,j,k,l=1\cdots\hat{A}\cdots N}} w_i w_j w_k w_l \times \frac{\left[\left(\mathbf{r}_{ij}\times\mathbf{r}_{kl}\right)\times\mathbf{r}_{il}\right]\left(\mathbf{r}_{ij}\times\mathbf{r}_{jk}\right)\left(\mathbf{r}_{jk}\times\mathbf{r}_{kl}\right)}{\left(r_{ij}r_{jk}r_{kl}\right)^n r_{il}^m}\right\}, \quad (6)$$

where A is a specific atom in a molecule. Knowledge of the individual atom contributions can help to identify which molecular substructures or terminal groups have the greatest influence on the overall chirality of the molecule.

The HTP of a chiral material is essentially a measure of its ability to rotate incident linearly polarized light as a function of its concentration (if it is dissolved in a LC host material) or as a function of path length (if it is pure LC material). The HTP ($\beta_{\mathbf{M}}$) is defined mathematically as

$$\beta_{\mathbf{M}} = \left(pc_W r\right)^{-1}, \quad (7)$$

where p is the pitch length of the chiral medium[39] (the distance needed for polarized light to rotate 360° through the medium), c_W is the weight concentration, and r is the enantiomeric purity of the chiral material. As Eq. (7) shows, a material with a large HTP will be more effective at rotating plane-polarized light at much lower concentrations (or shorter path lengths) than a material with a small HTP. Materials with a large HTP are also more desirable because they can be used in much lower concentrations to achieve an equivalent optical effect, which not only reduces materials and device costs (chiral materials are usually the most expensive component of an LC mixture), but also avoids potential solubility and miscibility problems that occur when higher concentrations of chiral dopants with a small HTP are used.

Recent work by Neal *et al.*[39] shows a good correlation between HTP and G_{0S}. The correlation between G_{0S} and HTP has also been validated by the research of Osipov and Kuball,[40] which lays the foundation for the relationship between CD and HTP. Circular dichroism is observed when an optically active material absorbs left- and right-hand circular polarized light differently as a function of wavelength. The correlation between G_{0S} and HTP was shown to be applicable only to rigid molecular systems.[39]

For flexible molecules, the scaled chirality index only accounts for one of many possible conformational isomers ("conformer") of a molecule. Thus, in molecules with a high degree of rotational freedom, a new method has been developed to account for a large number of conformers. This method defines a complex chirality parameter χ_0 based on the Connoly[41] surface of a chiral molecule. This parameter, which can be computed very rapidly, has been used most effectively in conjunction with a Monte Carlo simulation.[42] In the simulation, a molecule is moved stepwise into millions of different conformations and the parameter is calculated for each conformer. Through this computationally intensive method, the prediction of HTP has been extended to flexible molecules in a limited number of cases.[43]

In the bulk of the previous literature on scaled chirality index calculations, the weight factor (w_i) is set to 1.0 to create a uniform density distribution. When using this method, it has been shown through the analysis of individual atom contributions that the main contributors to G_{0S} are (1) atoms located at points of steric stress and (2) atoms located a large distance from the molecular core (these are most frequently hydrogen atoms). Only one other weighting method has ever been applied. Solymosi *et al.*[44] set the weight of each atom equal to its van der Waals volume in their study of ferroelectric LC systems. This weighting method took into account the effect of excluded volume and was appropriate for use in the prediction of spontaneous polarization.

Our approach substituted the atomic mass into the calculation as the weight (w_i = atomic mass), as first suggested by Solymosi *et al.*[38] To our knowledge, we were the first to use atomic mass as the weighting factor for the chirality index.[41] We hypothesized that the application of atomic mass would negate the effects of distance from the molecular core and enhance the effects of steric stress. Because the atoms at the greatest distance from the core are usually hydrogen and those at points of steric stress are carbon and/or other heavier elements, appropriate weighting was expected to enhance the accuracy of the chirality index and lead to a greater predictive power for important properties like HTP.

Briefly stated, the calculation of the scaled chirality index involves a series of five steps: (1) The desired molecular structure is created and energy minimized using conventional molecular mechanics computational software. (2) All possible groups of four neighboring atoms within the molecule are selected and used to form the corners of a tetrahedral symmetry element. (3) The edge lengths of each tetrahedron are calculated and put into the chirality index equation to compute the chirality for a given tetrahedral element. (4) Summing all tetrahedral element contributions to the chirality gives the overall chirality index (no contributions from symmetric tetrahedra). (5) A scaling factor is applied to compensate for the variation in the number of tetrahedral symmetry elements as a function of molecular size. In our case, the *actual mass of each atom in every tetrahedral element* is taken into account, yielding the *weighted, scaled chiral index* G_{0SW}.

The effectiveness of the new weighted, scaled chirality index calculation was tested by calculating the HTP for six well-known rigid and flexible chiral molecular systems (binaphthol derivatives, helicenes, chiral steroid esters, phenylpropanoic acid derivatives, and mono- and bis-aminoanthraquinones with chiral substituents)[41] and comparing the calculated data to experimental HTP data from the literature.[45–52] A Pearson correlation of the calculated HTP data to the experimental HTP data was determined for each molecular system and as a global correlation for all systems. The Pearson correlation r is a measure of the fit of a least squares linear regression through the data set. Likewise, the correlation coefficient R^2 describes the proportion of the points that can be accounted for by the linear regression. For rigid molecular systems, the overall correlation was very strong for both the unweighted and weighted chirality indices, as shown by the linear regression fit for the plots of the chiral indices versus the experimental HTP data in Fig. 106.57.[41] Although these molecules are all relatively rigid, the most flexible molecules within the systems appear to have the poorest correlation to experimental HTP data. A close examination of individual atom contributions reveals the benefits that the weighting system was expected to provide: the hydrogen atoms are not large contributors and the effects of steric stress are pronounced. The use of atomic mass predicts HTP more accurately when the experimental HTP is higher than 100 μm^{-1}. In the case of the flexible systems, although the overall correlations were not as strong (as was expected to be the case from previous work by Neal *et al.*),[39] the use of atomic mass to weight the chirality index did enhance the

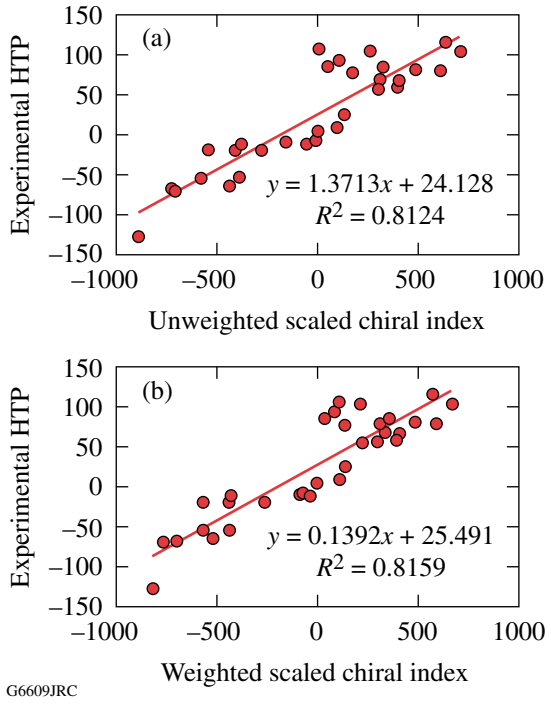

Figure 106.57
The weighted (a) and unweighted (b) scaled chiral indices of all 32 rigid molecules plotted against the experimental helical twisting power data. A linear regression is used to determine the strength of the correlation. The R^2 value of the weighted index (0.82) is slightly stronger than that of the unweighted index (0.81).

quality of the correlation between calculated and experimental results significantly.[41]

With the effectiveness of the new chirality index method now established, we applied it to the calculation of weighted and scaled chirality indices for the enantiomerically enriched nickel dithiolenes described previously in **Enantiomerically Enriched Nickel Dithiolene Complexes** (p. 117) and shown in Table 106.XIII. This chirality index data was then used to calculate the theoretical HTP for each chiral metal complex.[41] The results of these calculations, along with available experimental HTP data, are shown in Table 106.XVI. Each X group can contain 1 to 3 chiral centers for a total of 4 to 12 chiral centers in each molecule. The rigid correlation was used both for the first two compounds where there was no spacer group ($n = 0$) and for all compounds with $n \leq 6$, while the flexible correlation was used for compounds with $n > 6$. For the materials with spacer groups, their low melting points made their purification very difficult and, as a result, sufficient quantities of high-purity materials were not available for experimental determination of the HTP.

Comparison of the calculated HTP values for the compounds in Table 106.XVI that contain a spacer group predicts that for materials with the same terminal X group, the HTP is expected to decrease with increasing spacer length. When the flexible spacer length is nine, the calculated HTP values are all generally the same. There is also good agreement between the calculated and experimental values for HTP in the two compounds with no spacer group, which, to a very limited extent, verifies the predictive capability of the approach. A full assessment of the predictive capabilities of the weighted, scaled chirality index requires isolation and purification, in sufficient quantities, of the remaining chiral nickel dithiolenes in Table 106.XVI for experimental HTP studies. This effort is currently in progress.

Because G_{0S} can fluctuate dramatically on the basis of the lowest energy state of the energy-minimized conformer,

Table 106.XVI: The chiral X groups and helical twisting power data for a series of nickel dithiolene IR dyes.

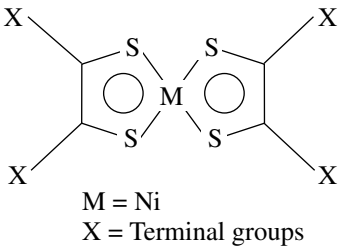

Terminal group	Experimental solvent	Experimental wavelength (nm)	Calculated wavelength (nm)
X = H	Hexane	720	720.91
X = CH_3	$CHCl_3$	774	843.08
X = CF_3	Pentane	715	775.05
X = S-C_4H_9	$CHCl_3$	1104	1012.31
X = C_6H_5	$CHCl_3$	866	845.19
X = 2-napthyl	$CHCl_3$	905	993.08
X_1, X_4 = H X_2, X_3 = C_6, H_5	CH_2Cl_2	805	857.78

extreme care must be taken when attempting to use the chirality index as a global predictor for HTP. The high dependence of G_{0S} on the minimum conformer energy state also accounts for the poor correlation of the scaled chirality index for flexible molecules. In this case, the computed energy-minimized conformer structure may not completely represent the actual conformer structure (or structures) that would be most likely to occur in nature. A better method for the prediction of HTP would take into account the many possible conformational geometries of a given molecule when computing the chirality through the use of Monte Carlo simulations.

Another limitation of the scaled chirality index method in its present form is that it is capable of accounting for factors such as temperature or dopant/host interactions only in nematic LC hosts. An improved chirality index that can incorporate both of these factors for other LC hosts would allow for a more accurate correlation, including global correlations between different molecular systems.[53] If the weighted, scaled chirality index method can be combined with a Monte Carlo simulation of geometric conformers (currently limited by processor speed), this enhanced chirality index could significantly increase the efficiency of chiral materials development. The latter point is the focus of our current and ongoing investigations.

Summary

Transition metal dithiolenes offer exciting new research opportunities in both materials chemistry and device applications. These new dyes are highly soluble in LC hosts, possess excellent thermal and photochemical stability, have structure-dependent dichroism, and can show LC mesomorphism on their own with the proper terminal functional groups. These properties, combined with their broad wavelength range, are all valuable attributes for near-IR LC device applications. The addition of enantiomerically enriched terminal groups to the dithiolene core results in a novel family of near-IR dyes that have low melting points (in many cases well below room temperature) and can induce both chirality and optical absorption when added to a nematic LC material. This new class of "liquid chiral dyes" is expected to give rise to a host of application possibilities in areas such as nonlinear optics and sensor protection.

The application of computational chemistry techniques to transition metal dithiolenes as described in this work represents a substantial technical achievement, given the lack of previous research activity in modeling transition metal organic complexes in general. The computational modeling methodology that we have developed was successfully applied to nickel dithiolene systems in the prediction of both the near-IR electronic absorbance spectra and (for enantiomerically enriched materials) the helical twisting power in a host medium. These calculations represent what we believe to be the first of this type attempted for nickel dithiolene systems, or, for that matter, in any other transition metal organometallic complex. With these new computational techniques now in hand, the concept of designing and predicting, prior to synthesis, which structural elements will provide the most promising new transition metal dithiolene complexes for optical and photonics applications now becomes a very realistic objective.

ACKNOWLEDGMENT

This work is supported by the U.S. Department of Energy Office of Inertial Confinement Fusion under Cooperative Agreement No. DE-FC52-92SF19460 and the University of Rochester. The support of DOE does not constitute an endorsement by DOE of the views expressed in this article.

REFERENCES

1. H. Suzuki and G. Hayashi, U.S. Patent No. 4,763,966 (15 July 1985).
2. K. Drexhage and U. Mueller-Westerhoff, U.S. Patent No. 3,743,964 (3 July 1973).
3. J.-F. Bai *et al*., J. Mater. Chem. **9**, 2419 (1999).
4. C. S. Winter *et al*., Mol. Cryst. Liq. Cryst. **235**, 181 (1993).
5. H. Tanaka *et al*., Science **291**, 285 (2001).
6. K. Wang and E. I. Stiefel, Science **291**, 106 (2001).
7. K. L. Marshall and S. D. Jacobs, Mol. Cryst. Liq. Cryst. **159**, 181 (1988).
8. K. L. Marshall, M. J. Guardalben, S. M. Corsello, M. S. Moore, I. A. Lippa, and R. P. Brecker, presented at the 16th Interdisciplinary Laser Science Conference (ILS-XVI), Providence, RI, 22–26 October 2000.
9. U. T. Mueller-Westerhoff *et al*., Mol. Cryst. Liq. Cryst. Lett. **56**, 249 (1980).
10. K. Ohta *et al*., Mol. Cryst. Liq. Cryst. **147**, 15 (1987).
11. U. T. Mueller-Westerhoff, B. Vance, and D. I. Yoon, Tetrahedron **47**, 909 (1991).
12. P. Espinet *et al*., Coord. Chem. Rev. **117**, 215 (1992).
13. U. T. Mueller-Westerhoff and B. Vance, in *Comprehensive Coordination Chemistry: The Synthesis, Reactions, Properties, and Applications of Coordination Compounds*, 1st ed., edited by Sir G. Wilkinson, R. D. Gillard, and J. A. McCleverty (Pergamon Press, Oxford, England, 1987), Vol. 2, pp. 595–631.
14. K. L. Marshall, B. Schudel, and I. A. Lippa, in *Liquid Crystals VII*, edited by I.-C. Khoo (SPIE, Bellingham, WA, 2003), Vol. 5213, pp. 201–212.

15. M. Colvin, Lawrence Livermore National Laboratory, Continuum Models of Solvation, 2000, http://gutenberg.llnl.gov/~colvin/solvation/solv.html (10 January 2000).
16. C. E. A. Wainwright and A. E. Underhill, Mol. Cryst. Liq. Cryst. **234**, 193 (1993).
17. N. Svenstrup *et al*., Synthesis **8**, 809 (1994).
18. A. Charlton *et al*., J. Mater. Chem. **4**, 1861 (1994).
19. K. L. Marshall, B. Klehn, B. Watson, and D. W. Griffin, in *Advanced Characterization Techniques for Optics, Semiconductors, and Nanotechnologies*, edited by A. Duparré and B. Singh (SPIE, Bellingham, WA, 2003), Vol. 5188, pp. 48–60.
20. *LLE Review Quarterly Report* **81**, 37, Laboratory for Laser Energetics, University of Rochester, Rochester, NY, LLE Document No. DOE/SF/19460-335 (1999).
21. K. B. Wiberg, *Physical Organic Chemistry* (Wiley, New York, 1964).
22. W. J. Hehre, *A Guide to Molecular Mechanics and Quantum Chemical Calculations* (Wavefunction, Irvine, CA, 2003).
23. W. J. Hehre, *Ab Initio Molecular Orbital Theory* (Wiley, New York, 1986).
24. C. C. J. Roothaan, Rev. Mod. Phys. **23**, 69 (1951).
25. P. M. W. Gill, Aust. J. Chem. **54**, 661 (2001).
26. W. J. Hehre *et al*., J. Chem. Phys. **52**, 2769 (1973).
27. M. S. Gordon *et al*., J. Am. Chem. Soc. **100**, 2670 (1978).
28. M. M. Francl *et al*., J. Chem. Phys. **77**, 3654 (1982).
29. M. Häser and R. Ahlrichs, J. Comput. Chem. **10**, 104 (2004).
30. R. M. Shroll and W. D. Edwards, Int. J. Quantum Chem. **63**, 1037 (1997).
31. E. R. Davidson, J. Comput. Phys. **17**, 87 (1975).
32. H. Zabrodsky and D. Avnir, J. Am. Chem. Soc. **117**, 462 (1995).
33. L. N. Lisetskii, Ukr. Fiz. Zh. **27**, 1321 (1982).
34. G. S. Chilaya and L. N. Lisetski, Mol. Cryst. Liq. Cryst. **140**, 243 (1986).
35. L. A. Batrachenko and L. N. Lisetskii, Zh. Strukt. Khim. **32**, 146 (1991).
36. H. Zabrodsky, S. Peleg, and D. Avnir, J. Am. Chem. Soc. **114**, 7843 (1992).
37. M. A. Osipov, B. T. Pickup, and D. A. Dunmur, Mol. Phys. **84**, 1193 (1995).
38. M. Solymosi *et al*., J. Chem. Phys. **116**, 9875 (2002).
39. M. P. Neal *et al*., J. Chem. Phys. **119**, 3567 (2003).
40. M. A. Osipov and H.-G. Kuball, Eur. Phys. J. E **5**, 589 (2001).
41. A. G. Noto and K. L. Marshall, in *Liquid Crystals IX*, edited by I.-C. Khoo (SPIE, Bellingham, WA, 2005), Vol. 5936, pp. 157–163.
42. D. J. Earl and M. R. Wilson, J. Chem. Phys. **120**, 9679 (2004).
43. D. J. Earl, Phys. Rev. E **71**, 021706 (2005).
44. M. Solymosi *et al*., Ferroelectrics **227**, 169 (2002).
45. N. Ferrarini *et al*., Liq. Cryst. **24**, 219 (1998).
46. D. J. Earl and M. R. Wilson, J. Chem. Phys. **119**, 10,280 (2003).
47. H.-G. Kuball *et al*., Mol. Cryst. Liq. Cryst. **352**, 195 (2000).
48. M. J. Cook and M. R. Wilson, J. Chem. Phys. **112**, 1560 (2000).
49. F. Brandenburger *et al*., Liq. Cryst. **28**, 1035 (2001).
50. Y. Aoki *et al*., Mol. Cryst. Liq. Cryst. **346**, 35 (2000).
51. Y. Aoki *et al*., Bull. Chem. Soc. Jpn. **71**, 2219 (2001).
52. H.-G. Kuball *et al*., J. Mater. Chem. **5**, 2167 (1995).
53. H. Kamberaj *et al*., Mol. Phys. **102**, 431 (2004).